fractal and fractional

Article

Influence of Geotextile Materials on the Fractal Characteristics of Desiccation Cracking of Soil

Binbin Yang [1,2], Shichong Yuan [2,*], Zhenzhou Shen [3] and Xiaoming Zhao [1,4]

1 School of Civil Engineering, Xuchang University, Xuchang 461000, China
2 School of Resources and Geosciences, China University of Mining and Technology, Xuzhou 221116, China
3 Yellow River Institute of Hydraulic Research, Zhengzhou 450003, China
4 College of Civil and Transportation Engineering, Hohai University, Nanjing 210098, China
* Correspondence: yuanshichong@cumt.edu.cn

Abstract: In recent years, the irregular cracks formed during the damage evolution of civil engineering materials have been able to be quantitatively described by using fractals. In this study, the fractal characteristics of the desiccation cracking of soil were investigated under different substrate contact and permeability conditions through a natural drying test in the laboratory. Three kinds of base contact conditions of soil, namely, grease, geomembrane, and geotextile, were designed, and two samples for each contact condition, including one parallel sample, were used. The continuous drying experiment was carried out at a constant ambient temperature. The crack morphology under different spacings was analyzed quantitatively using digital image processing technology. The fractal dimensions of three soil substrate contact conditions (grease, geomembranes, and geotextiles) were between 1.238 and 1.93. When the crack network on the soil surface stops developing, the fractal dimensions under the three experimental conditions are 1.88, 1.93 and 1.79, respectively. In the final state of crack development, the crack intensity factor of the sample with grease at the bottom is 2.99% and 4.02% higher than that of the sample with geomembranes and geotextiles at the bottom, respectively. The residual water contents of the samples with bottom contact conditions of grease, geomembrane, and geotextile increase successively, which are 3.12%, 5.76% and 9.71%, respectively. The effects of interface friction and permeability on soil cracking behavior are analyzed, and the evolution characteristics and formation mechanisms of cracks in soil are revealed.

Keywords: fractal characteristics; desiccation cracking; geotextile materials; soil surface

check for updates

Citation: Yang, B.; Yuan, S.; Shen, Z.; Zhao, X. Influence of Geotextile Materials on the Fractal Characteristics of Desiccation Cracking of Soil. *Fractal Fract.* **2022**, *6*, 628. https://doi.org/10.3390/fractalfract6110628

Academic Editor: Wojciech Sumelka

Received: 3 October 2022
Accepted: 26 October 2022
Published: 28 October 2022

1. Introduction

Fracture media have good fractal characteristics. The fractal dimension of the fracture body, surface fractal dimension, and axis fractal dimension can greatly reduce the complexity and dispersion of the test process. Under the action of an arid climate, the soil will have significant shrinkage deformation and cracking, which will directly lead to natural disasters such as land subsidence and water and soil loss, and have a great negative impact on the stability of surface infrastructure and underground engineering structures [1,2]. In many parts of the world, large-scale cracking and damage of infrastructure such as houses, roads, and bridges have occurred due to severe drought, resulting in huge economic losses [3,4]. China is a country with the most serious extreme climate events and disasters in the world, and there are many kinds—high-intensity, high-frequency, and serious harm [5,6]. The research data of the China Meteorological Administration show that the frequency and scope of extreme weather events such as mass or regional high temperatures, rainstorms, and droughts will increase significantly, and that the disaster risk will increase for a long time in the future. Especially in recent decades, the number and scale of major engineering construction projects in China have been increasing [7,8]. Drought extreme climate events will lead to geological disasters by affecting major engineering facilities themselves and important auxiliary facilities, especially the engineering geological environment relied upon by major projects, thus further affecting the safety, stability, reliability, and durability of the project; it also has an important impact on the operation efficiency and economic benefits of major projects.

Extreme arid climate disasters change the surface rock and soil temperature field, structure field, and material field, especially the water field, through various action modes, and then they change the engineering geological characteristics of the rock and soil mass, and cause disasters [9]. The continuous water evaporation caused by an arid climate will also lead to the development of a large number of dry shrinkage cracks in the soil, commonly known as cracking, which greatly weaken the engineering properties of the soil and provide favorable conditions for the development of soil engineering disasters [10,11]. In recent years, a large number of scholars and research institutions at home and abroad have begun to pay attention to the cracking behavior of soil under extreme arid climate conditions [12–14]. The cracking of the soil surface will multiply the permeability of soil, and will have a negative impact on hydraulic engineering and environmental geotechnical engineering [15]. In 2007, the severe drought in Chongqing caused serious cracking and reduced the stability of more than 1200 reservoir dams in the region, which directly faced the threat of dam failure after rainstorms. The same problem also occurred in hundreds of kilometers of flood control dams in Britain, the Netherlands, the United States, Australia and many other countries, with tens of billions of dollars needing to be invested every year to check and to repair the cracks developed in the dam body, to prevent piping and collapse. Cracking will greatly weaken the mechanical properties of soil [16,17]. Under the action of an arid climate, expansive soil will have a large degree of shrinkage deformation, and a large number of cracks easily develop on the surface. Swelling shrinkage and fissure are the typical characteristics of expansive soil. Therefore, expansive soil is often called "cracked soil". The middle route of the South-to-North Water Transfer Project in China crosses the expansive soil canal section for nearly 400 km. Most of the canal section collapses, and shallow landslides are related to the cracks developed in the expansive soil, especially under the repeated action of cracking in the dry season and water expansion in the rainy season, resulting in the unsaturated process of the soil and the expansion of the unsaturated zone, which greatly changes the physicochemical, hydraulic, and mechanical properties of the soil [18]. Under the action of an arid climate, the surfaces of some soil cultural relics or ancient buildings are also easy to develop and crack, so as to accelerate the weathering, denudation, and destruction of the surface structure, which greatly increases the difficulty of the protection of cultural relics and ancient sites. In the design of municipal solid waste sanitary landfill, there are many examples of the cracking failure of the isolation system due to the insufficient consideration of arid climate factors. Some scholars have pointed out that drought evaporation has led to more loose and broken surface source deposits, which have created convenient conditions for the outbreak of large-scale debris flow in the rainy season [19,20].

In order to evaluate soil evaporation behavior, based on the classical water heat air transport theory, different scholars have proposed different evaporation models to predict and evaluate soil evaporation under atmospheric action, such as the Penman model, the Philip and De Vries model, and the modified Penman Wilson model [21,22]. These classical theoretical models can generally obtain good calculation results in homogeneous sand, but there will be large errors in clay, mainly because the interaction between clay and water molecules is very complex, and because the water migration process in clay under evaporation is much more complex than that in sand [23]. Most of the existing theoretical models only consider ambient temperature, relative humidity, and other meteorological parameters. Less consideration is given to the influence of soil factors on evaporation and the change in soil engineering properties caused by evaporation, which greatly restricts the popularization and application of the above theoretical results in practical engineering.

In order to study soil cracking, many scholars have proposed different methods in the past, and have basically established the cracking research method system, which is mainly divided into three categories: the indoor model test, the in situ observation test, and numerical simulation [24–26]. The quantitative acquisition of geometric parameters of the crack network has always been an important aspect of crack research. It is of great significance to evaluate the crack development state, engineering properties, and potential impact of soil. The early quantitative analysis technology of cracking is mainly based on on-site manual measurement, but the measurement results are easily disturbed by human and environmental factors. In addition, the geometry of the crack network is extremely complex; thus, it is difficult to obtain accurate and comprehensive parameters such as crack length, width, area, and angle in the actual operation process [27]. Miller et al. [28] introduced the crack strength factor parameter, which is defined as the ratio of the crack area to the total soil area. Velde [29] analyzed the fractal dimension of fractures using digital image processing technology. In recent years, with the development of computer science, image processing technology has been widely used in the quantitative analysis of the crack network. The development degree of soil and concrete cracking can be described by fractal [30].

However, there are few reports on the relationship between soil drying shrinkage cracking, and the friction and permeability of the contact surface. Therefore, in order to fully understand the influence of interface friction and water permeability on soil drying cracking behavior, six samples were prepared in the laboratory. The basic conditions of the substrate were grease, geomembranes, and geotextiles. They were continuously dried at a constant ambient temperature. Using digital image processing technology, crack morphology under different spacing is described quantitatively. The effects of interface friction and permeability on soil cracking behavior are analyzed, and the evolution characteristics and formation mechanism of cracks in soil are revealed.

2. Materials and Methods

2.1. Materials

The soil used in this experiment was from Urumqi, Xinjiang, China. It has a continental arid climate in the middle temperate zone, with less rain and sufficient sunshine. The average annual precipitation is less than 200 mm. The hottest months of the year are July and August, with an average temperature of 25.7 °C. The coldest month is January, with an average temperature of −15.2 °C. In recent years, various construction projects have been accelerating. The sedimentary depth of the test soil is 50~75 cm, and the main mineral components are illite, illite montmorillonite interlayer minerals, and kaolinite. After the test soil is taken back to the laboratory, it needs to be dried at 110 °C for 48 h, and then it is stored in a sealed bottle after grinding and a 2 mm screen. The grease used in this experiment is milky white and viscous. It was purchased from Lingcheng Lubricating Oil Co., Ltd. in Xinxiang City, China. Its temperature range is −30~180 °C. In the industry, it has lubrication, rust prevention, anti-corrosion, and anti-oxidation effects. Its main component is fatty acid lithium soap thickening refined mineral oil, and many additives such as anti-oxidation and anti-rust agents are added. The geomembranes used in this experiment were black, with a thickness of 0.2 mm, a relative density of 0.918~0.965, and a melting point of 110~130 degrees. Additionally, a high-density polyethylene impermeable membrane material was used. The breaking strength of the material was greater than 20.0 KN/m, and the strength retention rate of the material was greater than 85.0% when it was soaked in a solution with pH of 2~11. The geotextiles used in this experiment were gray-white, 2 mm thick, with good water permeability on one side, a strong tensile force, and corrosion resistance.

2.2. Sample Preparation

The prepared soil was fully mixed with distilled water to prepare saturated mud with a water content of 130%. The mud was placed on a shaking table and vibrated for 5 min to remove bubbles in the mud. Six round glass containers were used to hold the mud, with an inner diameter of 20 cm and a height of 4 cm. Grease was applied to the bottom of the container to reduce the floor roughness during mud drying shrinkage. The sample numbers were S1 and S2, where S2 was a parallel sample. Geomembranes and geotextiles were cut into regular circles with a radius of 10 cm and were placed at the bottom of the glass container. The samples were numbered S3, S4, S5 and S6, where S4 and S6 were parallel samples. Then, the saturated mud was carefully poured into containers, and the weight of the mud in each container was about 300 g. The sample preparation process and image processing process are shown in Figure 1. Table 1 summarizes the parameter information of the test samples.

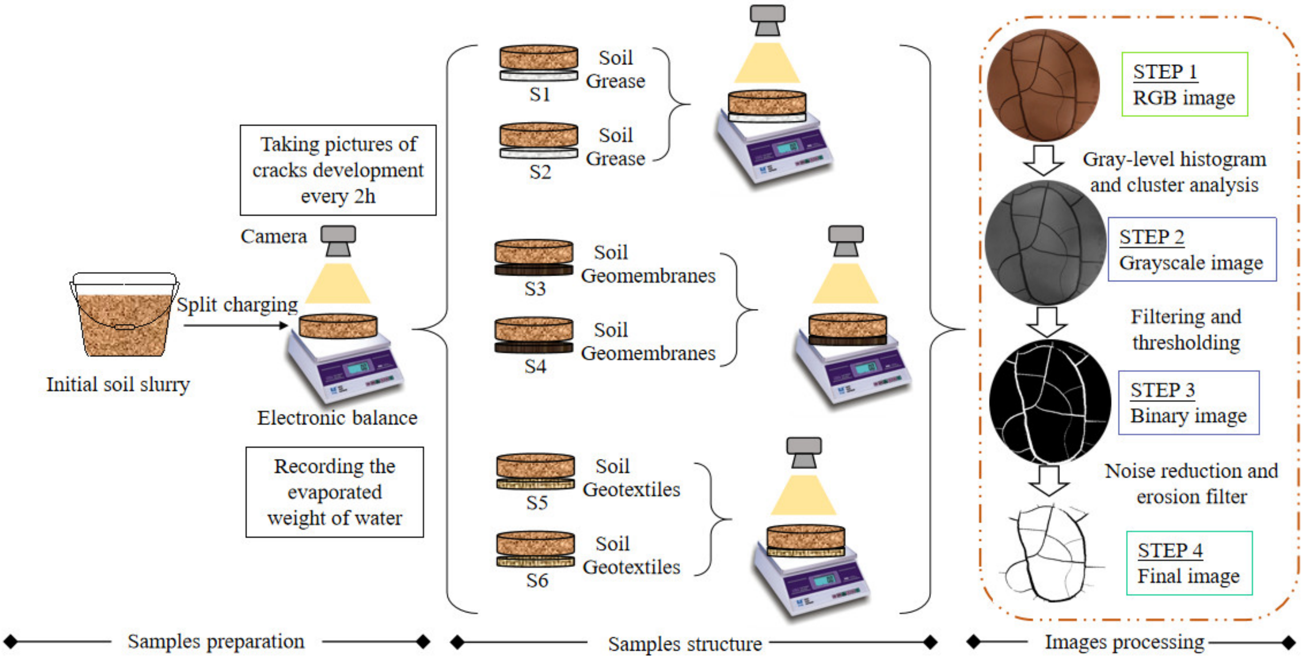

Figure 1. Schematic view of the testing procedure and image processing.

Table 1. The parameters of each group of specimens.

Specimen No.	Interfacial Friction Condition	Interfacial Permeability Condition	Weight of Slurry (g)
S1	Grease	Impervious	300
S2	Grease	Impervious	300
S3	Geomembranes	Impervious	300
S4	Geomembranes	Impervious	300
S5	Geotextiles	Permeable	300
S6	Geotextiles	Permeable	300

2.3. Test Method and Image Processing

The prepared test samples were evaporated and dried in a constant temperature and humidity test chamber; the temperature was controlled at 25 °C, and the relative humidity was 30%. The samples were weighed at different time intervals, accurate to 0.01 g, to determine the change in the moisture content during drying. The dynamic process of sample surface drying cracking was monitored with a digital camera. The crack propagation was quantitatively analyzed via image processing technology. When the mass change for the sample within one day was less than 0.01 g, the drying test was stopped.

The image of the fracture development process was processed, and then, the fracture was quantitatively analyzed. In quantitative analysis, only the edge shrinkage area of the container boundary may be mistaken for soil cracks, resulting in an increase in geometric parameters such as the total length and the average width of the cracks. In order to reduce the influence of the edge shrinkage region on determining the geometric parameters of the crack network, only the central part was used, $\Pi \times 10$ cm^2, for quantitative analysis. The process of the image processing is shown in Figure 1. The original color image was first converted to a gray image. In order to enhance the contrast between the crack and the surrounding soil matrix, the homomorphic filtration method was adopted. Then, a Gaussian filter was used to denoise the image. Upon analyzing the pixels of the gray image, gray values of the soil and background that were greater than the threshold of 255 were specified as 0, and gray values of the crack component that were less than the threshold were specified as 1. The filtered gray image was converted into a binary image. Finally, two quantitative parameters, the fracture rate and the fractal dimension of the fracture network, were obtained.

2.4. Crack Characteristics

Various methods have been proposed to calculate the lengths of cracks, such as using observations in convex windows proposed by Kulatilake and Wu [31]. Therefore, circular windows are used, which improves the estimation of the true trace length distribution of cracks [32–35]. However, the use of circular windows is more accurate than observations in convex windows. Therefore, circular windows have been used to estimate the true trace lengths of cracks [36]. The fractal dimension is an important parameter for quantitatively characterizing the fractal nature of objects, and can be used to comprehensively describe the degree of cracking of soils [37,38]. In fractal dimension analyses, the dimension of a straight-line segment is defined as 1, with a length of X. By dividing the line into $N = b$ smaller segments of equal length, each smaller segment is a point of the straight-line segment. Each point is identical to the entire line, and this ratio is known as the similarity ratio r, where $r = 1/b = 1/N$. In two-dimensional space, there are $N = b^2$ small squares, which are similar to the entire two-dimensional plane, thus satisfying:

$$\begin{cases} (k-1)X/b \leq x < kX/b, (k = 1, 2, \ldots b) \\ (h-1)Y/b \leq y < kY/b, (k = 1, 2, \ldots b) \end{cases} \tag{1}$$

The similarity ratio is given by:

$$r(N) = 1/b = 1/N^{(1/2)} \tag{2}$$

Similarly, the similarity ratio for a D_s-dimension cylinder is given by:

$$r(N) = 1/N^{(1/D)} \tag{3}$$

Then,

$$\begin{cases} Nr^{D_s} = 1 \\ \log r(N) = \log(1/N^{1/D_s}) = -\log N/D_s \\ D_s = -\log N/\log r(N) = \log N/\log(1/r) \end{cases} \tag{4}$$

where N is the number of units which resembles the entire crack image, r is a coefficient of the similarity ratio, and D_s is the fractal dimension from the crack image.

The crack intensity factor R_t is defined as the ratio of the projected area of the crack on the 2D plane to the total 2D surface area. It represents the space occupied by the crack of the specimen. It can be used to describe the degree of cracking as follows:

$$R_t = \frac{S_{crack}}{S_{soil}} \tag{5}$$

where S_{crack} is the projected area of the crack and S_{soil} is the total surface area of the sample.

The evaporation rate E is the weight of water lost per unit time, which can be calculated using Formula (1) according to the change in the recorded sample weight data. The evaporation rate can be calculated using Equation (3).

$$E = \frac{\Delta m}{\Delta t \cdot S_E} \quad (6)$$

where Δt is the time of evaporation, Δm is the amount of evaporated water, and S_E is the area of the sample.

3. Results

3.1. Fractal Characteristics of Soil Cracks Due to Geotextile Materials

When the moisture content of the sample decreased to a certain value due to continuous evaporation, cracks began to appear on the surface of the soil sample. Taking samples S1, S3, and S5 as an example, the crack initiation and propagation processes are illustrated (Figure 2). The crack modes of sample S1 at different water contents are shown in Figure 2. The water content of sample s1-1 when cracks began to appear was about 64.2%. After the first crack appeared, several independent cracks initiated and propagated on the sample surface. When the water content of the sample was relatively high, these initial independent cracks were defined as first-order cracks. With the progress of evaporation, the initial crack expanded and terminated after intersecting. When the water content reached about 24.6%, the initial crack network divided the sample surface into several soil blocks. With a further reduction in the water content, some new cracks were generated in these soil blocks or existing primary cracks, and the soil blocks were divided into smaller blocks. Compared with the primary cracks, these cracks were later formed at relatively low water contents and had smaller widths and lengths; these are called secondary cracks. With a further decrease in the water content, cracks with smaller visibilities and lengths appeared, which are called tertiary cracks. The final crack morphology after drying shows that the intersection of crack segments almost formed "T" and "+" shapes, indicating that the cracks were usually perpendicular to each other. Most clods were quadrilateral, with a few being pentagonal.

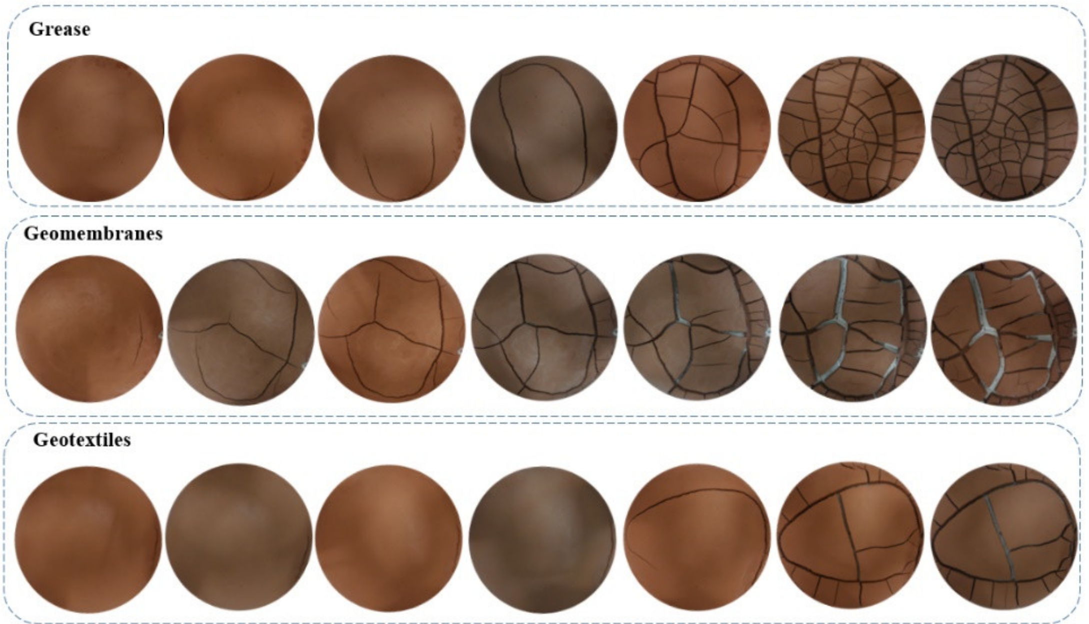

Figure 2. Development process of cracks in samples.

Figure 3 shows the variation process of the fractal dimension with evaporation duration during the development of sample surface cracks under different test conditions. The dry shrinkage fracture network formed on the soil surface had good statistical self-similar classification characteristics. The fractal dimensions of three soil substrate contact conditions (grease, geomembranes, and geotextiles) were between 1.238 and 1.93. When the crack network on the soil surface stopped developing, the fractal dimensions under the three experimental conditions were 1.88, 1.93 and 1.79, respectively. When the substrate contact condition was geomembranes, it had the largest fractal number, and when the substrate contact condition was geoextensions, it had the smallest fractal number. From the final state, when the contact condition of the soil substrate was geotextiles, the final fractal dimension was reduced by 4.79% and 7.25%, compared with the other two contact conditions.

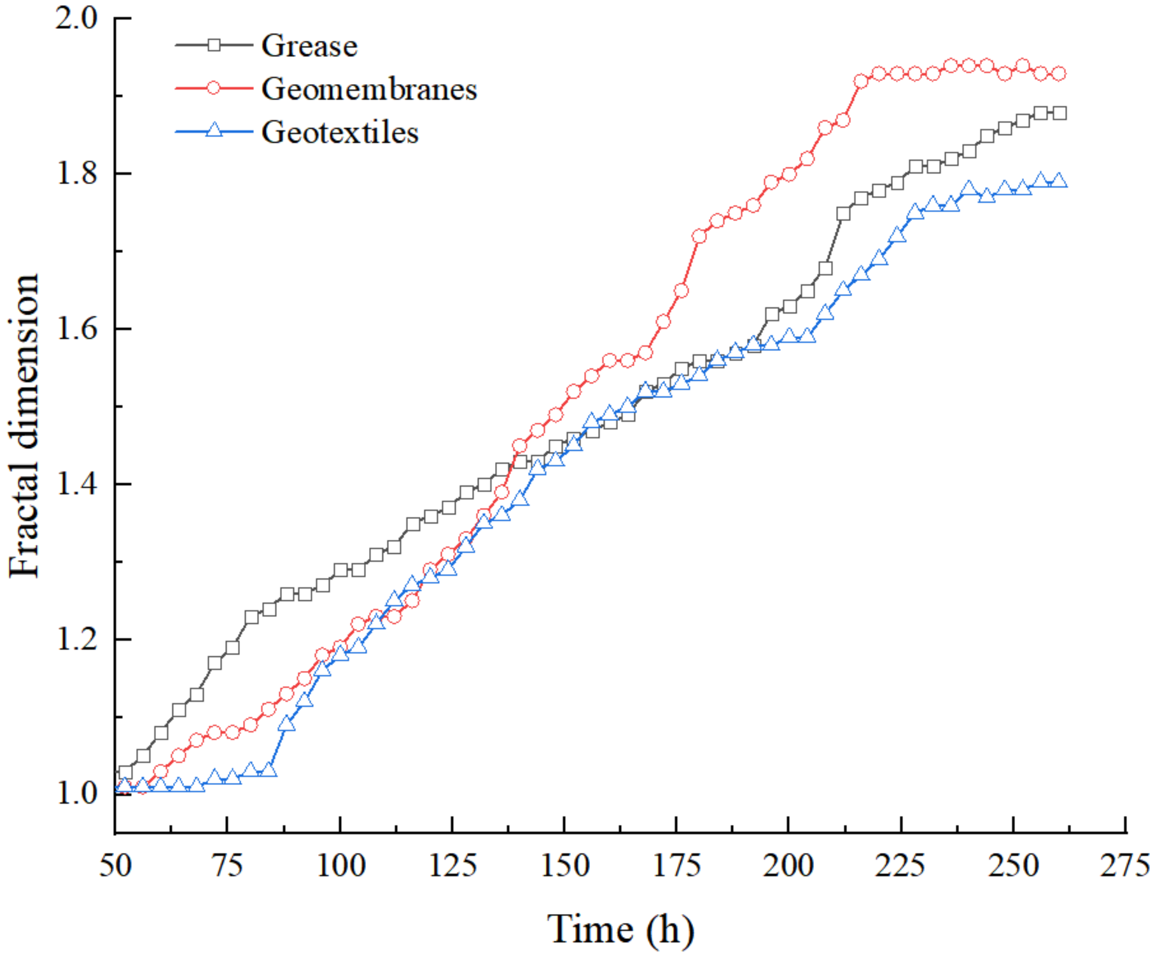

Figure 3. Fractal dimensions of soil samples with grease, geomembranes, and geotextiles over time.

Figure 4 shows the variation in the crack intensity factor (CIF) with evaporation duration during the development of surface cracks of samples under different test conditions. The crack intensity factors of samples with grease placed at the bottom were always greater than those of samples with geomembranes and geotextiles placed at the bottom throughout the development of fractures. Additionally, in the final state, the CIF of the sample with grease at the bottom was 2.99% and 4.02% higher than the crack intensity factors of the samples with geomembranes and geotextiles at the bottom, respectively. In the process of fracture development, the crack intensity factor of the sample with grease at the bottom was always the smallest, but after the fracture development stopped, the crack intensity factor was 1.03% higher than that of the sample with geotextiles at the bottom.

3.2. *Evaporation Characteristics of Soil Due to Geotextile Materials*

Figure 5 shows the change in water content and evaporation rate over time for the sample with grease, geotextiles, and geomembranes at the bottom of the sample. As shown in Figure 5, the water content of the six samples decreased with time. According to the variation law of evaporation curves, the evaporation process of the sample can be divided into three stages, stage I: constant rate stages of evaporation, stage II: deceleration rate stages of evaporation, and stage III: residual rate stages of evaporation. The evaporation curve can be well fitted using the Boltzmann function. Stage I of the samples with grease and geomembranes at the bottom is roughly the same, with both being greater than 40 h. However, the evaporation curve stage I of the samples with geotextiles lasts the shortest, at only 28 h. Similarly, the durations of stage II of the evaporation curves of the samples with increase, geomembranes, and geotextiles at the bottom were successively shortened, at 115 h, 112 h, and 108 h, respectively. In addition, the residual water content of stage III represents the water holding capacity of the soil sample under drought conditions. The residual water contents of the samples with grease, geomembranes, and geotextiles at the bottom increased successively, being 3.12%, 5.76%, and 9.71%, respectively. Compared with the contact condition with grease at the bottom, the residual water content of the samples with geomembranes and geotextiles at the bottom increased by 84.62% and 211.21%, respectively. However, the first crack occurred at approximately the same time in all of the samples. In this study, the time at which the first crack on the sample surface reached a length of about 2 mm (which can be accurately seen by the naked eye or digital camera) was defined as the cracking time.

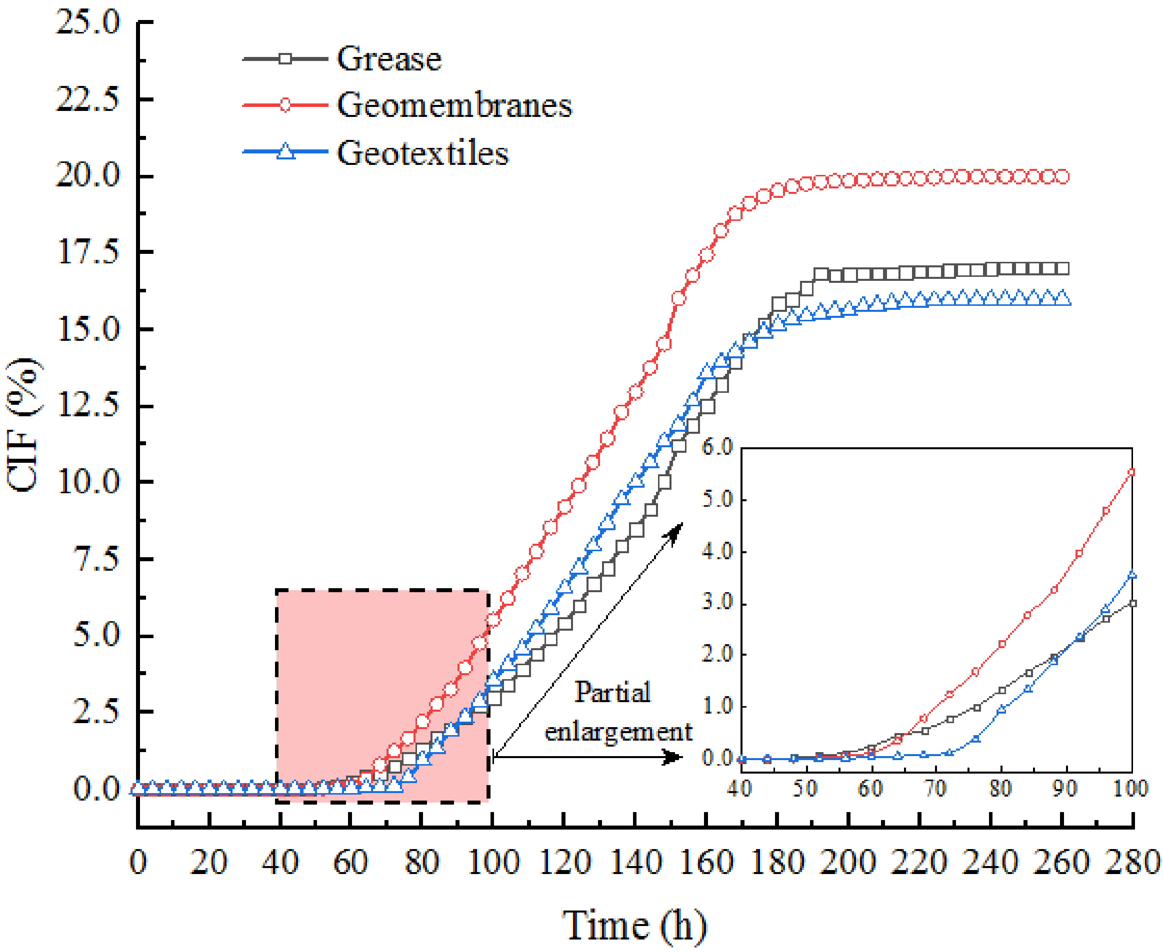

Figure 4. Crack intensity factor of soil samples with grease, geomembranes, and geotextiles versus time.

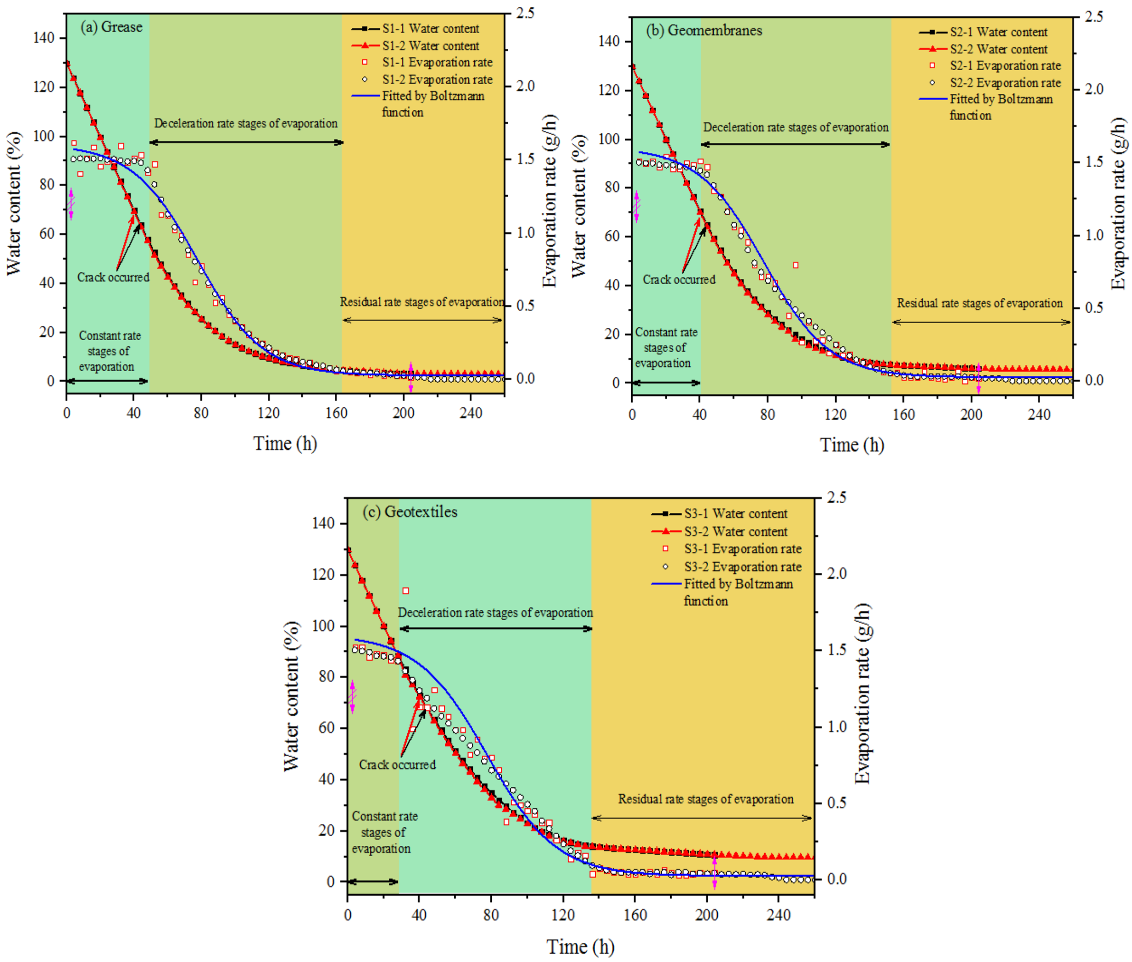

Figure 5. Water content and evaporation of soil samples versus time. (**a**) Grease, (**b**) geomembranes, (**c**) geotextiles.

4. Discussion

During the drying process, due to the continuous evaporation of water in the soil, the soil water content and saturation gradually decrease, resulting in a gradual increase in matrix suction and tensile stress in the soil. There is a positive correlation between the tensile strength and the matrix suction of soil. Once the tensile stress generated in the soil exceeds the tensile strength of the soil, cracks will occur on the surface of the sample. The distribution of the tensile stress depends not only on the defects in the soil, but also on the base friction. When the sample base is composed of grease, the friction of the sample base is significantly less than that for when the sample base is geomembranes. When the sample substrate is grease or geomembranes, the substrate is impervious. In the process of the gradual dehydration and drying of the sample, the shrinkage of the sample with friction in the horizontal direction will be limited, which makes it more difficult for the soil particles to become close to each other. In this case, the tensile stress may transfer and lead to dry cracking. The interlayer friction has a constraint on the movement of the soil particles, and a greater constraint on the movement of the soil particles. This will lead to a faster concentration of tensile stress, and increase the propagation rate and crack intensity factor of soil cracks. Therefore, reducing the friction of the sample substrate can reduce the dry cracks on the sample surface.

Through a large number of indoor experiments on soil drying and cracking, it is found that most soil samples are placed in impermeable plastic or glass containers at the bottom. However, the water permeability condition of the sample substrate is also an important factor affecting the surface drying and cracking of soil samples. In this experiment, when the soil sample base is grease and geomembranes, the base is impervious, while when the sample base is geotextiles, the base of the soil sample is permeable. At this time, the sample can dry and lose water from the top, sides, and bottom. The bottom of the soil sample is also the water loss area; therefore, when the base contact condition is geotextiles, the initial water loss rate of the soil sample is relatively fast, and the cracking rate of the surface is relatively large. However, because geotextiles have a certain degree of water absorption, the final soil moisture content in the final state will be higher than that in the other two soils. The soil cracking mechanism under different substrate friction and permeability conditions is shown in Figure 6.

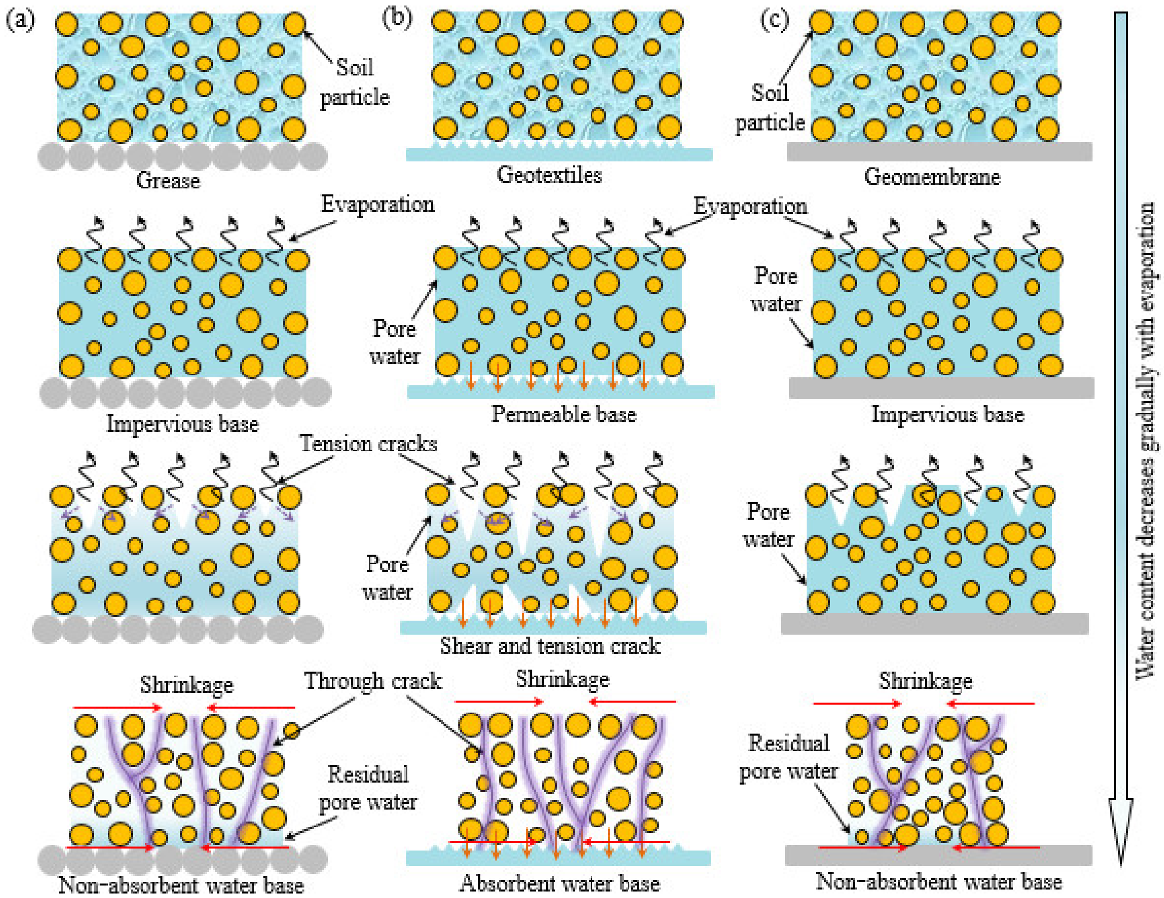

Figure 6. Soil cracking mechanism under different substrate friction and permeability conditions. (**a**) Grease, (**b**) geotextiles, (**c**) geomembranes.

5. Conclusions

In order to investigate the development of desiccation cracks in soils affected by different geomembrane materials, free drying tests were carried out in the laboratory. The characteristics of the desiccation cracks of soil were determined for different amounts of water loss. The characteristics of the progressive changes in the cracks were quantitatively analyzed using digital image processing.

An important factor affecting the drying and cracking of the soil sample surface is the water permeability of the sample matrix. The dry shrinkage fracture network formed on the soil surface has good statistical self-similar classification characteristics. In the process of the gradual dehydration and drying of the sample, the shrinkage of the sample with friction in the horizontal direction will be limited, which makes it more difficult for the soil particles to become close to each other. Therefore, reducing the friction of the sample substrate can reduce the dry cracks on the sample surface.

Due to the water absorption of geotextiles, when the base of the sample is geotextiles, the base of the soil sample is permeable. At this time, the sample can be dried from the top, sides, and bottom. The bottom of the soil sample is also the water loss area; therefore, the base is geotextiles, the initial water loss rate of the soil sample is relatively fast, and the cracking rate of the surface is relatively large.

According to the variation law of the evaporation curve, the evaporation process of the sample can be divided into three stages. Stage I: constant rate stages of evaluation. Stage II: degradation rate stages of evaluation. Stage III: residual rate stages of evaluation. The evaporation curve can be well fitted using the Boltzmann function.

Author Contributions: Data curation, Formal analysis, Writing—original draft, B.Y.; Investigation, Methodology, Writing—review and editing, S.Y.; Supervision, Resources, Funding acquisition, Z.S.; Software, Validation, Visualization, X.Z. All authors have read and agreed to the published version of the manuscript.

Funding: This research was funded by the Natural Science Foundation of Henan (222300420281) and the National Natural Science Foundation of China (U2243210).

Institutional Review Board Statement: Not applicable.

Informed Consent Statement: Not applicable.

Data Availability Statement: All data, models, or code generated or used during the study are available from the corresponding author upon reasonable request.

Acknowledgments: The authors would like to thank all the anonymous referees for their constructive comments and suggestions.

Conflicts of Interest: The authors declare no conflict of interest.

References

1. Al Qadad, A.; Shahrour, I.; Rouainia, M. Influence of the soil-atmosphere exchange on the hydric profile induced in soil-structure system. *Nat. Hazards Earth Syst. Sci.* **2012**, *12*, 2039–2049. [CrossRef]
2. Sen, Z. Water structures and climate change impact: A review. *Water Resour. Manag.* **2020**, *34*, 4197–4216. [CrossRef]
3. Belloulid, M.O.; Hamdi, H.; Mandi, L.; Ouazzani, N. Solar greenhouse drying of wastewater sludges under arid climate. *Waste Biomass Valoriz.* **2017**, *8*, 193–202. [CrossRef]
4. Tang, C.; Zhu, C.; Cheng, Q.; Zeng, H.; Xu, J.; Tian, B.; Shi, B. Desiccation cracking of soils: A review of investigation approaches, underlying mechanisms, and influencing factors. *Earth Sci. Rev.* **2021**, *216*, 103586. [CrossRef]
5. Dai, A. Drought under global warming: A review. *WIREs Clim. Chang.* **2011**, *2*, 45–65. [CrossRef]
6. Kang, Y.; Khan, S.; Ma, X. Climate change impacts on crop yield, crop water productivity and food security—A review. *Prog. Nat. Sci. Mater. Int.* **2009**, *19*, 1665–1674. [CrossRef]
7. Sun, Y.; Zhang, X.; Zwiers, F.; Song, L.; Wan, H.; Hu, T.; Yin, H.; Ren, G. Rapid increase in the risk to extreme summer heat in Eastern China. *Nat. Clim. Chang.* **2014**, *4*, 1082–1085. [CrossRef]
8. Xu, K.; Yang, D.; Yang, H.; Li, Z.; Qin, Y.; Shen, Y. Spatio-temporal variation of drought in China during 1961–2012: A climatic perspective. *J. Hydrol.* **2015**, *526*, 253–264. [CrossRef]
9. Naviglio, D.; Formato, A.; Scaglione, G.; Montesano, D.; Pellegrino, A.; Villecco, F.; Gallo, M. Study of the grape cryo-maceration process at different temperatures. *Foods* **2018**, *7*, 107. [CrossRef]
10. Xu, J.J.; Zhang, H.; Tang, C.S.; Cheng, Q.; Liu, B.; Shi, B. Automatic soil desiccation crack recognition using deep learning. *Geotechnique* **2022**, *72*, 337–349. [CrossRef]
11. Li, D.; Yang, B.; Yang, C.; Zhang, Z.; Hu, M. Effects of salt content on desiccation cracks in the clay. *Environ. Earth Sci.* **2021**, *80*, 671. [CrossRef]
12. Levatti, H.U. Numerical solution of desiccation cracks in clayey soils. *Encyclopedia* **2022**, *2*, 1036–1058. [CrossRef]
13. Izzo, M.Z.; Miletić, M. Desiccation cracking behavior of sustainable and environmentally friendly reinforced cohesive soils. *Polymers* **2022**, *14*, 1318. [CrossRef] [PubMed]
14. Ralaizafisoloarivony, N.; Degré, A.; Mercatoris, B.; Leonard, A.; Toye, D.; Charlier, R. Assessing soil crack dynamics and water evaporation during dryings of agricultural soil from reduced tillage and conventional tillage fields. *Proceedings* **2019**, *30*, 59. [CrossRef]
15. Deng, Y.F.; Yue, X.B.; Cui, Y.J.; Shao, G.H.; Liu, S.Y.; Zhang, D.W. Effect of pore water chemistry on the hydro-mechanical behaviour of Lianyungang soft marine clay. *Appl. Clay Sci.* **2014**, *95*, 167–175. [CrossRef]
16. Wang, L.; Li, G.; Li, X.; Guo, F.; Tang, S.; Lu, X.; Hanif, A. Influence of reactivity and dosage of MgO expansive agent on shrinkage and crack resistance of face slab concrete. *Cem. Concr. Compos.* **2022**, *126*, 104333. [CrossRef]

17. Colombi, T.; Kirchgessner, N.; Iseskog, D.; Alexandersson, S.; Larsbo, M.; Keller, T. A time-lapse imaging platform for quantification of soil crack development due to simulated root water uptake. *Soil Tillage Res.* **2021**, *205*, 104769. [CrossRef]
18. Guo, J.; Dai, Z.; Li, S.; Muhammad, N.; Gao, H. Study on creep characteristics of expansive soil in high-fill channel of south-to-north water transfer project. *Adv. Civ. Eng.* **2020**, *2020*, 8852131. [CrossRef]
19. Dong, M.; Hu, H.; Guo, Q.; Gong, X.; Azzam, R.; Kong, M. Correlation of environmental parameters and the water saturation induced deterioration of earthen archaeological sites: The case of world heritage Liangzhu city, China. *Heritage* **2021**, *4*, 387–400. [CrossRef]
20. Zhao, G.; Ren, K.; Ma, Q. Research on collapse failure process and mechanism of Earthen sites under the action of capillary water. *Appl. Mech. Mater.* **2013**, *438–439*, 1226–1231.
21. Camillo, P.J.; Gurney, R.J. A resistance parameter for bare-soil evaporation models. *Soil Sci.* **1986**, *141*, 95–105. [CrossRef]
22. Wilson, G.; Fredlund, D.; Barbour, S. Coupled soil-atmosphere modelling for soil evaporation. *Can. Geotech. J.* **1994**, *31*, 151–161. [CrossRef]
23. Song, W. Experimental Investigation of Water Evaporation from Sand and Clay Using an Environmental Chamber. Ph.D. Thesis, Université Paris-Est, Paris, France, 2014.
24. Liu, C.; Tang, C.S.; Shi, B.; Suo, W.B. Automatic quantification of crack patterns by image processing. *Comput. Geosci.* **2013**, *57*, 77–80. [CrossRef]
25. Albrecht, B.; Benson, C. Effect of desiccation on compacted natural clays. *J. Geotech. Geoenviron. Eng.* **2001**, *127*, 67–75. [CrossRef]
26. Konrad, J.; Ayad, R. A idealized framework for the analysis of cohesive soils undergoing desiccation. *Can. Geotech. J.* **1997**, *34*, 477–488. [CrossRef]
27. Wang, L.; Yu, Z.; Liu, B.; Zhao, F.; Tang, S.; Jin, M. Effects of fly ash dosage on shrinkage, crack resistance and fractal characteristics of face slab concrete. *Fractal Fract.* **2022**, *6*, 335. [CrossRef]
28. Miller, C.; Mi, H.; Yesiller, N. Experimental analysis of desiccation crack propagation in clay liners. *J. Am. Water Resour. Assoc.* **1998**, *34*, 677–686. [CrossRef]
29. Velde, B. Structure of surface cracks in soil and muds. *Geoderma* **1999**, *93*, 101–124. [CrossRef]
30. Wang, L.; Huang, Y.; Zhao, F.; Huo, T.; Chen, E.; Tang, S. Comparison between the influence of finely ground phosphorous slag and fly ash on frost resistance, pore structures and fractal features of hydraulic concrete. *Fractal Fract.* **2022**, *6*, 598. [CrossRef]
31. Kulatilake, P.H.S.W.; Wu, T.H. Estimation of mean trace length of discontinuities. *Rock Mech. Rock Eng.* **1984**, *17*, 215–232. [CrossRef]
32. Mauldon, M. Estimating mean fracture trace length and density from observations in convex windows. *Rock Mech. Rock Eng.* **1998**, *31*, 201–216. [CrossRef]
33. Mauldon, M.; Dunne, W.M.; Rohrbaugh, M.B., Jr. Circular scanlines and circular windows: New tools for characterizing the geometry of fracture traces. *J. Struct. Geol.* **2001**, *23*, 247–258. [CrossRef]
34. Wang, L.; Zhou, S.; Shi, Y.; Huang, Y.; Zhao, F.; Huo, T.; Tang, S. The influence of fly ash dosages on the permeability, pore structure and fractal features of face slab concrete. *Fractal Fract.* **2022**, *6*, 476. [CrossRef]
35. Zhang, L.; Einstein, H.H. Estimating the intensity of rock discontinuities. *Int. J. Rock Mech. Min. Sci.* **2000**, *37*, 819–837. [CrossRef]
36. Sturzenegger, M.; Stead, D.; Elmo, D. Terrestrial remote sensing-based estimation of mean trace length, trace intensity and block size/shape. *Eng. Geol.* **2011**, *119*, 96–111. [CrossRef]
37. Mandelbrot, B.B. Self-affine fractal sets, I: The basic fractal dimensions. In *Fractals in Physics, Proceedings of the Sixth Trieste International Symposium on Fractals in Physics, Trieste, Italy, 9–12 July 1985*; Elsevier: Amsterdam, The Netherlands, 1986; pp. 3–15.
38. Mandelbrot, B.B. Self-affine fractal sets, II: Length and surface dimensions. In *Fractals in Physics, Proceedings of the Sixth Trieste International Symposium on Fractals in Physics, Trieste, Italy, 9–12 July 1985*; Elsevier: Amsterdam, The Netherlands, 1986; pp. 17–20.